High resolution measurements of the ^{241}Am(n,2n) reaction cross section

C. Sage,[1,2,3,4,*] V. Semkova,[2,5] O. Bouland,[3,6] P. Dessagne,[4] A. Fernandez,[7] F. Gunsing,[1] C. Nästren,[7] G. Noguère,[3] H. Ottmar,[7] A. J. M. Plompen,[2] P. Romain,[8] G. Rudolf,[4] J. Somers,[7] and F. Wastin[7]

[1]*Commissariat à L'Energie Atomique Saclay, DSM/IRFU/SPhN, F-91191 Gif-sur-Yvette, France*

[2]*European Commission, Joint Research Centre, Institute for Reference Materials and Measurements, Retieseweg 111, B-2440 Geel, Belgium*

[3]*Commissariat à L'Energie Atomique Cadarache, DEN/CAD/DER/SPRC/LEPh, F-13108 St Paul-lez-Durance, France*

[4]*Institut Pluridisciplinaire Hubert Curien, F-67037 Strasbourg, France*

[5]*Institute for Nuclear Research and Nuclear Energy, Bulgarian Academy of Sciences, BG-1784 Sofia, Bulgaria*

[6]*Los Alamos National Laboratory, Theoretical Division, Los Alamos, New Mexico 87545, USA*

[7]*European Commission, Joint Research Centre, Institute for Transuranium Elements, Postfach 2340, D-76125 Karlsruhe, Germany*

[8]*Commissariat à L'Energie Atomique, DAM, DIF, F-91297 Arpajon, France*

(Received 6 July 2009; published 4 June 2010)

Measurements of the ^{241}Am(n,2n) reaction cross section have been performed at the Joint Research Centre (JRC) Geel in the frame of a collaboration between the European Commission (EC) JRC and French laboratories from CNRS and the Commissariat à L'Energie Atomique (CEA) Cadarache. Raw material coming from the Atalante facility of CEA Marcoule has been transformed by JRC Karlsruhe into suitable $^{241}AmO_2$ samples embedded in Al_2O_3 matrices specifically designed for these measurements. The irradiations were carried out at the 7-MV Van de Graaff accelerator. The ^{241}Am(n,2n) reaction cross section was determined relative to the ^{27}Al(n,α)^{24}Na standard cross section. The measurements were performed in four sessions, using quasi-monoenergetic neutrons with energies ranging from 8 to 21 MeV produced via the ^{2}H(d,n)^{3}He and the ^{3}H(d,n)^{4}He reactions. The induced activity was measured by standard γ-ray spectrometry using a high-purity germanium detector. Below 15 MeV, the present results are in agreement with data obtained earlier. Above 15 MeV, these measurements allowed the experimental investigation of the ^{241}Am(n,2n) reaction cross section for the first time. The present data are in good agreement with predictions obtained with the TALYS code that uses an optical and fission model developed at CEA.

DOI: 10.1103/PhysRevC.81.064604 PACS number(s): 25.40.Fq, 25.45.−z, 25.60.Dz

I. INTRODUCTION

Accurate neutron-induced reaction cross-section data are required for many practical applications, especially to predict reliably the behavior of reactor cores in both present and future fission reactors. Because the nucleus ^{241}Am is one of the most abundant isotopes in spent nuclear fuel, as well as one of the most highly radiotoxic among the actinides, accurate data are required to study the possible transmutation of long-lived radioactive waste with advanced high-neutron-energy reactors.

The determination of the (n,2n) reaction cross section for actinides is difficult. A neutron multiplicity experiment has to exclude neutrons produced in fission events. In the case of the ^{241}Am isotope, the cross section for fission (3 b) is much higher than that for the (n,2n) reaction (250 mb at most) and an accurate subtraction of the fission contribution would be required to obtain the (n,2n) yield. A measurement of prompt γ rays would lead to an underestimation of the cross section due to internal conversion and would make it impossible to observe the direct population of the ground state. The activation method avoids these problems but is applicable to only a few actinides on account of constraints imposed by the natural activity, availability, and purity of the sample material. As a result, relatively few actinide (n,2n) data are known well enough to provide good tests for model estimates. The nucleus ^{241}Am is one of those few for which the activation technique can be used, because of the short-lived reaction product ^{240}Am ($T_{1/2}$ = 50.8 h) emitting an interference-free high-energy γ ray with a high probability after β-decay. The main problem consists in the important ^{241}Am natural activity, with especially the strong 60 keV and a multitude of higher-energy γ rays.

Two references report measured cross sections for the ^{241}Am(n,2n) reaction at neutron energies around 14 MeV [1,2], and two recent works report data for neutron energies from threshold to 14 MeV [3,4]. At 14 MeV, the data of Refs. [2,4] are in good agreement, whereas the data from Ref. [1] appear to be systematically lower, agreeing only within one to two standard deviations with the other works. The data of Refs. [3,4] agree well below 10 MeV but reveal huge discrepancies around 11 MeV. Estimates of the cross section available from applications libraries show a large spread in the predicted excitation function [5–7] (see Fig. 1 and also Ref. [4]). Measurements at higher incident neutron energies are thus needed to guide evaluations and model calculations.

In the present work, the cross section of the ^{241}Am(n,2n) reaction has been measured for the first time above 15 MeV. Results are shown for six energies from 16.1 to 20.6 MeV. In addition, measurements are reported for three energies below 15 MeV to check the consistency of our work against the existing data. The results are compared with the above-mentioned estimates from the recent evaluated data libraries

*sagechristophe@yahoo.fr

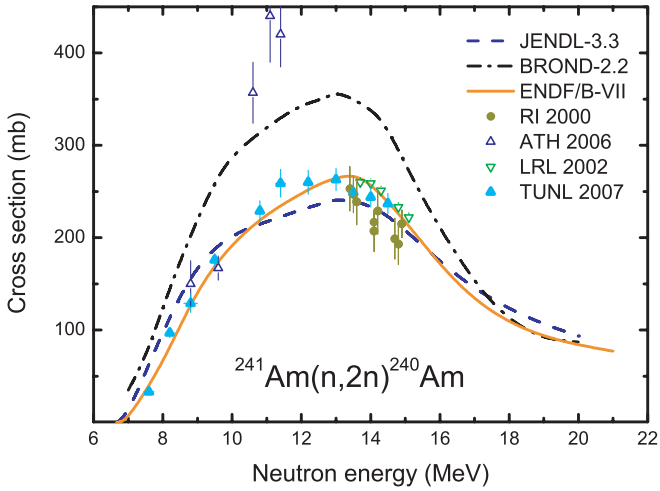

FIG. 1. (Color online) Status of the ^{241}Am$(n,2n)$ cross-section data and evaluations. See Refs. [5] for ENDF/B-VII, [6] for JENDL-3.3, and [7] for BROND-2.2. Not shown are data from Ref. [8] (JEFF-3.1), because this library adopted the estimates from Ref. [6]. Data tables for the works shown were obtained from Ref. [9].

and a new estimate that was made with the aid of the TALYS code [10,11], employing a physical model that was tuned to reproduce all available experimental information for neutron-induced reactions on ^{241}Am. Some details about the model calculations for this excitation function are given.

II. EXPERIMENTAL PROCEDURE

The reported cross sections were measured with the activation technique. Here, details of the sample preparation, the irradiations, and the activity determinations are described. The data analysis procedure is presented in Sec. III and some explanations about the nuclear model calculations in Sec. IV. The results, the experimental uncertainties, and their correlations are given in Sec. V.

A. Preparation of the samples

The samples were prepared by a method especially developed for the present study at the Joint Research Centre (JRC), Institute for Transuranium Elements (ITU), in Karlsruhe. This method is based on the production of porous alumina granules by powder metallurgy. The americium was introduced into the porous particles by infiltration of its nitrate solution. Following drying to eliminate water, and calcination to convert to oxide, the resulting powder was pressed into pellets of 12 mm diameter and 2 mm thickness. The sample weight was on average 400 mg and the average americium content was 40 mg. The americium-alumina composite was then encapsulated into aluminum containers.

The geometry of each sample was examined by x-ray radiography and the americium content determined by calorimetry [12]. The mass of ^{241}Am in the samples was also determined by γ spectrometry at the Institute for Reference Materials and Measurements (IRMM) with results agreeing within 2%.

TABLE I. Mass and elemental composition of the samples.

Sample number	Total mass (g)	^{241}Am content (mg)	Al_2O_3 (g)	Calculated ^{241}Am (wt %)
1	0.342	32.2 ± 0.1	0.305	9.43
2	0.442	42.2 ± 0.1	0.394	9.51
3	0.428	40.3 ± 0.1	0.382	9.42
4	0.435	41.0 ± 0.1	0.388	9.42
5	0.448	41.2 ± 0.1	0.401	9.20
6	0.447	42.1 ± 0.1	0.399	9.42

Table I summarizes the characteristics of the six samples produced for these measurements.

B. Irradiation setup

The irradiations were carried out at the 7-MV Van de Graaff accelerator at the IRMM using three different arrangements. First, quasi-mono-energetic neutrons with energies of 8.34 and 9.15 MeV were produced via the ^{2}H$(d,n)^3$He reaction ($Q = 3.269$ MeV) at $E_d = 5.5$ and 6.3 MeV, respectively, using a deuterium gas target. The target cell was 4 cm in length and 4 cm in diameter with a 5-μm molybdenum entrance window. The pressure in the cell was kept under 120 kPa. The samples were placed 1.5 cm from the target. Second, the ^{3}H$(d,n)^4$He reaction ($Q = 17.59$ MeV) was employed using a solid-state Ti/^{3}H target (2 mg/cm^2 thick) on a silver backing (0.4 mm thick) to produce quasi-mono-energetic neutrons with energies between 16.1 and 20.6 MeV. The samples were placed at 0° relative to the incident deuteron beam at 2 cm distance from the target. Finally, neutrons with $E_n = 13.3$ MeV were obtained using 1-MeV deuterons at 125° neutron emission angle. In this case the sample was placed 3.9 cm from the target.

In all cases, the sample was mounted in a specially prepared lightweight aluminum frame for safety reasons. The frame allowed foils of Al, Fe, In, Nb and Ni to be attached on both sides of the sample to monitor the neutron flux and to account for its variation with distance. The distance between the monitor foils and the sample was 3 mm in the front and 10 mm at the back. The typical beam current on the target was 10 μA, with a typical neutron flux of 5×10^7 neutrons s^{-1} cm^{-2} at this position. During the irradiations, each of which lasted 2 days on average, a BF_3 counter operated in multichannel-scaling acquisition mode was used to record the time profile of the neutron flux. This time profile allows for a correction that is important when beam current variations are substantial (see below).

C. Neutron energy and flux determination

The mean neutron energy and yield distributions as a function of deuteron energy and emission angle for the primary neutrons of the ^{2}H$(d,n)^3$He and ^{3}H$(d,n)^4$He reactions were calculated by the code ENERGYSET [13,14], which is based on the reaction cross-section evaluations of Ref. [15] and energy-loss estimates with stopping powers of Ref. [16]. The

neutron fluence rate was determined using the ^{27}Al$(n,\alpha)^{24}$Na standard cross section [17,18].

The presence of low-energy secondary neutrons necessitated the application of significant corrections to the measured activation yields for the reactions with low threshold energies. To account for this contribution, the neutron flux density distributions were determined using previously measured time-of-flight spectra combined with the spectral index method [19]. The latter involves various monitor reactions with distinct energy thresholds. The reactions used for the unfolding were ^{27}Al$(n,p)^{27}$Mg, ^{56}Fe$(n,p)^{56}$Mn, ^{115}In$(n,n')^{115m}$In, ^{27}Al$(n,\alpha)^{24}$Na, ^{93}Nb$(n,2n)^{92m}$Nb, and ^{58}Ni$(n,p)^{58m+g}$Co. The cross-section data for these dosimetry reactions were taken from Smith *et al.* [20] for the ^{115}In$(n,n')^{115m}$In reaction, from Wagner *et al.* [17] for the ^{27}Al$(n,\alpha)^{24}$Na and ^{93}Nb$(n,2n)^{92m}$Nb reactions, and from the ENDF/B-VI library [21] for the remaining reactions.

D. Induced activity measurements

After the irradiation, the induced activity was measured of-line by standard γ-ray spectrometry using a high-purity germanium (HPGe) detector. The data acquisition was controlled by the Maestro system supplied by Ortec, and the γ-ray spectra were analyzed using the software package Genie2000 of Canberra. The decay data for the monitor reactions were taken from Refs. [22–27] and are given in Table II along with the reaction Q values [28]. The decay data for ^{240}Am and ^{241}Am used for the data analysis were taken from Refs. [29,30] and are given in Table III.

A Pb/Sn/Cu shielding, with 5, 3, and 3 mm thicknesses, respectively, was used to reduce the important natural activity from the ^{241}Am decay to limit the dead time of the system to less than 15% (between 7% and 15%, typically, for a sample placed directly on top of the shielding). The correctness of the dead time given by the acquisition system was verified by a comparison of the counting rates from a ^{60}Co standard source with and without an Am sample. The detector was additionally shielded from the side with a 10-mm-thick Cu cylinder to avoid detection of scattered γ rays.

For the two main γ rays emitted in the decay of ^{240}Am (Table III), Fig. 2 clearly shows that the peak corresponding to the energy of 888.85 keV is contaminated by the natural activity of the sample itself while the γ ray with 987.79 keV is free from interference by the sample activity. The intensities of both the 888.85- and 987.79-keV γ lines were measured as a function of the cooling time after irradiation. The results confirm that the 987.79-keV γ line remains free of interference because the measured decay curve closely corresponds to that of ^{240}Am. As anticipated, this is not the case for the 888.85-keV γ ray. The increased background under the peaks in Fig. 2 concerns Compton events from the ^{24}Na activity produced by the ^{27}Al(n,α) reaction on the container and Al_2O_3 matrix.

The sample activities were determined using the counts in the full energy peak of the γ-ray transition. For this it was important to know the absolute peak efficiency and the energy calibration. Concerning the energy calibration, several single- and multi-γ-ray standard point sources were used, such as ^{241}Am (E_γ = 59.5 keV), ^{109}Cd (E_γ = 88 keV), ^{57}Co (E_γ = 122.1 and 136.5 keV), ^{137}Cs (E_γ = 661.66 keV), ^{54}Mn (E_γ = 834.8 keV), and ^{65}Zn (E_γ = 1115.5 keV). The calibration was made for different radial positions and detector-source distances. The efficiency of the detection setup was determined by a Monte Carlo simulation using the code MCNP5 [31] and taking into account the entire detection geometry. The

TABLE II. β-decay properties of the monitor reactions used for the neutron flux normalization (from Refs. [22–27]).

Reaction	Half-life of product	Q (MeV)	E_γ (keV)	Intensity (%)
^{27}Al$(n,p)^{27}$Mg	9.458(12) min	−1.828	843.8	71.8(4)
^{56}Fe$(n,p)^{56}$Mn	2.5789(1) h	−2.913	846.8	98.9(3)
^{115}In$(n,n')^{115m}$In	4.486(4) h	0.336	336.2	46(2)
^{27}Al$(n,\alpha)^{24}$Na	14.997(12) h	−3.132	1368.6	99.9936(15)
^{93}Nb$(n,2n)^{92m}$Nb	10.15(2) d	−8.967	934.4	99.07(4)
^{58}Ni$(n,p)^{58}$Co	70.86(7) d	0.401	810.8	99.45(1)

TABLE III. Relevant γ rays following the α-decay.

Nucleus	Half-life	E_γ (keV)	I_γ (%)
^{240}Am	50.8(3) h	987.79(6)	72.2(9)
		888.85(5)	24.7(5)
^{241}Am	432.6(6) yr	59.5409(1)	35.9(4)
		208.01(3)	7.91×10^{-4}(19)
		322.52(3)	1.52×10^{-4}(4)
		332.35(3)	1.49×10^{-4}(3)
		335.37(3)	4.96×10^{-4}(11)
		368.65(3)	2.17×10^{-4}(5)
		376.65(3)	1.38×10^{-4}(3)
		662.40(2)	3.64×10^{-4}(9)
		722.01(3)	1.96×10^{-4}(4)
		887.3(3)	2.2×10^{-7}(5)

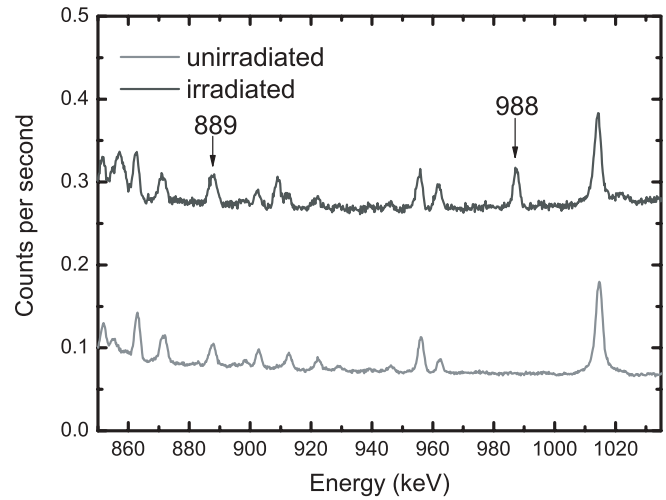

FIG. 2. High-energy part of the measured spectra for irradiated and unirradiated samples.

results of this simulation were compared with measured values and efficiency curves by fitting experimental points with polynomial logarithmic functions [32]. The detector geometry parameters have been optimized to obtain agreement between measurements and simulations within the uncertainty limits.

Corrections for photon absorption, including the disk shape of the samples and monitor foils, were calculated using the same MCNP5 simulation of the detection geometry. These corrections have been incorporated in the efficiency ϵ and were estimated to 0.2% and 1.3%, respectively.

Coincidence summings of γ rays also occurred for some of the monitor reactions and had to be corrected for using well-known methods described in Ref. [33] and detailed knowledge of individual γ-ray decay schemes obtained from Ref. [34]. This correction is as high as 25.4% for the ^{27}Al(n,α) ray at 1368.6 keV, 0.3% for the ^{27}Al(n,p) ray at 843.8 keV, 13.5% for the ^{58}Ni(n,p) ray at 810.8 keV, 0.4% for the ^{93}Nb$(n,2n)$ ray at 934.4 keV, and 9.9% for the ^{56}Fe(n,p) ray at 846.8 keV.

III. DATA ANALYSIS

A. Data analysis formalism

The data obtained from the present experiment were determined using the following expression:

$$\sigma_{\mathrm{Am}} = \sigma_{\mathrm{Al}} \frac{S_{\mathrm{Am}}}{S_{\mathrm{Al}}} \frac{[I\epsilon f_\Sigma f_r n\Phi_0]_{\mathrm{Al}}}{[I\epsilon f_\Sigma f_r n\Phi_0]_{\mathrm{Am}}} \prod_k \frac{C_{k,\mathrm{Am}}}{C_{k,\mathrm{Al}}}, \tag{1}$$

where σ_{Am} and σ_{Al} are the cross sections for the ^{241}Am$(n,2n)$ and ^{27}Al(n,α) reactions, S_{Am} and S_{Al} are the number of counts for the two reactions, I is the γ-ray emission probability (or intensity), ϵ is the absolute peak efficiency of the detector for the emitted γ ray, f_Σ and f_r are the time factors described below, n is the number of target nuclei, Φ_0 is the neutron flux, and C_k are the different correction factors.

According to Eq. (1), the cross sections σ_{Am} for the ^{241}Am$(n,2n)$ reaction are determined relative to the cross sections σ_{Al} of the ^{27}Al(n,α) reaction, which were obtained from Refs. [17,18]. The right-hand side of Eq. (1) further consists of three factors. The first is the ratio of counts observed for the two reactions. The second is a fraction with the main factors in an activation experiment and essentially corresponds to a zero-order approximation or a highly idealized experiment. The third factor is a product of ratios of correction factors that account for the deviations from the idealized case. The idealized case is defined in this section, and the corrections are presented and detailed in the next.

During irradiation, the number of product nuclei, $N(t)$, builds with time t according to

$$N(t) = ne^{-\lambda t} \int_E \sigma(E) \int_0^t \Phi(E,\tau) e^{\lambda\tau} d\tau dE, \tag{2}$$

where n is the number of target nuclei, σ is the reaction cross section, λ is the decay constant of the product nucleus, and $\Phi(E,t)$ is the time- and energy-dependent neutron flux per unit energy. It was assumed that no product nuclei are present at the start of irradiation. In our type of experiment, the number of target nuclei is not affected by the flux, as would be the case for a long irradiation in a reactor.

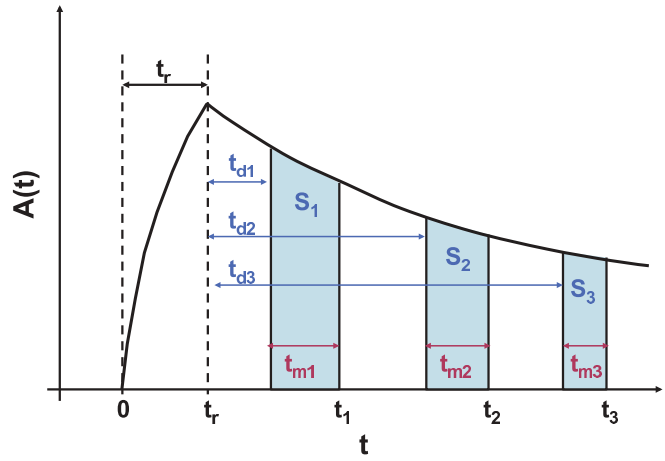

FIG. 3. (Color online) Schematic view of the successive activity measurements following an irradiation as a function of time.

In the ideal case, the flux is constant and monoenergetic and may be expressed as $\Phi(E,t) = \Phi_0\delta(E - E_0)$. This results in a number of product nuclei N_r at the end of irradiation at time t_r given by

$$N_r = N(t_r) = n\sigma(E_0)\Phi_0 \frac{f_r}{\lambda}, \tag{3}$$

where $f_r = 1 - e^{-\lambda t_r}$ is the irradiation time factor.

For the second step of the experiment (i.e., the activity measurement), we can write the number of events S registered in the HPGe detector during the successive measurements sessions, as illustrated in Fig. 3, as

$$S = \sum_i S_i = \lambda N_r I\epsilon f_\Sigma = n\sigma\Phi_0 f_r I\epsilon f_\Sigma, \tag{4}$$

where

$$f_\Sigma = \frac{1}{\lambda} \sum_i e^{-\lambda t_{d_i}} (1 - e^{-\lambda t_{m_i}}). \tag{5}$$

is the time factor taking into account the different measurements that last a time t_{m_i} and start after the time t_{d_i} relative to the end of irradiation.

The third expression on the right-hand side of Eq. (4) is obtained by substituting for N_r from Eq. (3). It shows explicitly how the ratio of observed counts $S_{\mathrm{Am}}/S_{\mathrm{Al}}$ is proportional to the cross-section ratio $\sigma_{\mathrm{Am}}/\sigma_{\mathrm{Al}}$, and inversion of the expression leads to Eq. (1) in the case of unit correction factors.

B. Corrections related to the irradiation process

For an actual experiment, corrections are needed to account for deviations from the ideal case both for the irradiations and for the activity determinations. The corrections C_k appear in Eq. (1) and were described in considerable detail for measurements at IRMM in Refs. [35–38]. They are applied for both the americium sample and the aluminum monitors and are either calculated in a rigorous way or small enough to be

treated as a perturbation. It may be noted that, unlike the above-mentioned references, corrections (geometry, self-attenuation, summing) required for the activity determination are described in Sec. II D and are lumped together in the detection efficiency.

For the irradiations, deuteron straggling in the target, the angle dependence of the neutron yield and energy, the close geometry, and multiple scattering of the neutron result in energy distributions of the primary component of the flux that differ for the monitor foils and the sample because of the flux attenuation between their different distances from the neutron source. This may be accounted for by simple means in very lightweight arrangements [37] or by more elaborate modeling using Monte Carlo simulations. The latter is essential for substantial sample masses and sizes [36]. Here, the ratio of the flux $\Phi_{0,\mathrm{Al}}/\Phi_{0,\mathrm{Am}}$ for the primary neutron component was determined by simulations of the flux attenuation using MCNPX [39]. The shape of the flux attenuation with distance r is assumed to be A/r^b, where $b = 2$ corresponds to the ideal case of a point source. The flux ratio is then equal to $(r_{\mathrm{Am}}/r_{\mathrm{Al}})^b$, with the two distances well known. From the simulation of the setup geometry, we can obtain the neutron flux as a function of the distance r from the target. Fitting this with the assumed function gives a factor b describing the flux attenuation ranging from 1.78 to 1.84, depending on the neutron energy.

The impact of fluctuations of the deuteron beam current during the 2-day-long irradiations were evaluated using the number of neutrons recorded by a BF_3 counter every minute. If we divide the total irradiation time t_r into m small time intervals Δt, the contribution for one single bin is proportional to $\Phi_i(1 - e^{-\lambda\Delta t})$, and the induced decay is proportional to $e^{-\lambda(m-i)\Delta t}$. The correction factor C_{flux} is then calculated as

$$C_{\mathrm{flux}} = \frac{\bar{\Phi}(1 - e^{-\lambda t_r})}{\sum_{i=1}^{m} \Phi_i(1 - e^{-\lambda\Delta t})e^{-\lambda(m-i)\Delta t}}, \qquad (6)$$

where $\bar{\Phi} = \sum \Phi_i/m$ is the average flux during the irradiation. The value of this correction factor ranges from 0.1% to 8.3% for the Am sample and from 0.7% to 31% for the Al foils, as can be seen in Table IV, and is strongly dependent on the beam stability condition during the 2-day-long irradiations. Because the time bins are very small, the correction can be considered exact and the associated uncertainty can be neglected.

TABLE IV. Flux fluctuation C_{flux} and low-energy neutrons C_{low} correction factors for each neutron energy.

Energy (MeV)	C_{flux}		C_{low}	
	Am	Al	Am	Al
8.34	0.9974	0.9925	1	1
9.15	1.0731	1.3117	1	1
13.33	0.9168	0.8288	1	1
16.10	1.0749	1.2335	1	1
17.16	0.9987	0.9878	0.998	0.997
17.90	0.969	0.933	0.998	0.997
19.36	1.0061	1.0157	0.941	0.926
19.95	0.9822	0.9433	0.922	0.891
20.61	0.9938	0.982	0.885	0.832

The last important correction is made because of the presence of low-energy breakup neutrons. Actually, these neutrons, which mainly come from secondary target reactions, were evaluated here using previously measured time-of-flight spectra of the neutron beam [38]. A cutoff energy E_c for each investigated secondary target reaction is defined below the quasi-mono-energetic neutron peak energy. The position of this cutoff varies depending on the incident deuteron energy and the reaction in question. The intensities of low-energy neutrons vary depending on the irradiation history of the target (deuterium buildup, oxidation, carbon deposits, and tritium loss). Therefore, the time-of-flight spectrum is divided in several groups for which the intensities relative to the primary neutrons are adjusted on the basis of the activities found in the monitor foils. The correction factor C_{low} is then calculated by forming the ratio of the sample activities produced by neutrons below the cutoff energy versus those produced by the entire neutron spectrum [35]. Both of these yields are calculated by integrating the product of the spectrum shape with assumed cross sections for the considered reactions. The correction factor is then derived from the expression

$$C_{\mathrm{low}} = 1 - \frac{\int_0^{E_c} \Phi(E)\sigma(E)dE}{\int_0^{\infty} \Phi(E)\sigma(E)dE}. \qquad (7)$$

The value of this correction factor ranges from 0.0% to 11.5% for the Am sample and from 0.0% to 17% for the Al foils. It is important to note that this factor varies in the same way for both the Am sample and the Al foils. Thus, the ratio of the factors ranges only from 0.0% to 6%, within a maximum uncertainty of 1.4% in the worst case.

In the case of the irradiations using a gas target (i.e., for the two lower-energy points), we calculated the background subtraction by simply comparing the gas-in and gas-out induced activities. The corresponding correction was very small and was neglected for the cross-section calculation. In addition, an estimate of the deuteron breakup contribution was made using the energy distribution and intensity data of Ref. [40]. This too turned out to be negligible on account of the low deuteron energy and the reaction thresholds.

IV. NUCLEAR MODEL CALCULATIONS

For the modeling of the ^{241}Am$(n,2n)$ reaction cross section, the TALYS [11] code was used. TALYS is a computer-code system for the prediction and analysis of nuclear reactions that involve neutrons, photons, protons, deuterons, tritons, helions, and α particles, in the 1 keV to 200 MeV energy range. Consistent calculations of all open channels above the resonance region are possible with this modern tool associated with a comprehensive parameter library. TALYS is built on a suite of three fundamental nuclear reaction models: optical, statistical, and pre-equilibrium.

For this work, the optical model calculations (of Bruyères-le-Châtel) were performed using [41–43] phenomenological dispersive optical model potentials for neutrons [and also for protons to treat charged particles (p,d,t,^{3}He,^{4}He) as combined in TALYS] validated over the 1 keV to 200 MeV energy range. These potentials are not implemented in TALYS but read as

external input. Because ^{241}Am is a deformed nucleus in its ground state, coupled-channels calculations, involving the first five states of the ground-state rotational band and the first three states of the lowest octupolar band as the coupling scheme [43], were achieved. At this stage, it is interesting to emphasize that the resulting total, reaction, and direct inelastic cross sections as well as neutron transmission coefficients are the primordial ingredients required for the next step in the calculation: the statistical compound nucleus emissions (taking into account a pre-equilibrium component when needed).

As a function of the neutron incident energy, the ^{241}Am$(n,2n)$ reaction cross section results from a balanced contribution of these two processes (compound and pre-equilibrium). Moreover, these two neutron emission processes are in competition with all other open channels that can occur in the studied energy range from the ^{241}Am$(n,2n)$ reaction threshold ($E^{n,2n}_{\text{threshold}} = 6.67$ MeV) up to 21 MeV: capture, inelastic, fission, and three-neutron emission (for energies above $E^{n,3n}_{\text{threshold}} = 12.65$ MeV). This means that we have to define the correct cross-section magnitudes of all these channels. The calculated capture cross section was fitted to the available experimental data by overruling the default renormalization to the s-wave strength function. Even if this channel has been taken into account, its contribution for the present study is not crucial (less than 2 mb above $E^{n,2n}_{\text{threshold}}$). In this aforementioned energy range, the ^{241}Am(n,n') inelastic component is the sum of three contributions: direct (from optical model calculations), compound, and pre-equilibrium. In fact, the compound inelastic component becomes rapidly negligible with increasing incident neutron energy: it contributes up to 50% to the inelastic cross section at $E^{n,2n}_{\text{threshold}}$, and it represents only around 1%, just 2 MeV above $E^{n,2n}_{\text{threshold}}$. Finally, to estimate the pre-equilibrium contribution, the default TALYS parameters for the pre-equilibrium (exciton) model [11] were retained.

For the fission channel, we used the double-humped (or triple-humped) fission barrier model implemented in TALYS (partly improved at Bruyères-le-Châtel [43,44]). For each hump, the transmission coefficient is the sum of all partial transmission coefficients related to each transition state with the same J^{π} and given by the Hill-Wheeler formula. This sum divides into two parts that represent the discrete and the continuum contributions of the transition states spectrum. The continuum part is obtained from an integration using the appropriate fission-level densities. Moreover, when the excitation energy of the compound nucleus (or of the residual nucleus contributing to the multichance fission) is lower than the barrier heights, fission transmission coefficients display a resonant structure because of the presence of nuclear excited levels in the second or third well (the so-called class II or III states) of the potential energy surface. In fact, it is more difficult to deal with the fission channel in a consistent way. Indeed, the fission parameters have to be adjusted previously for the first-chance fission before adjusting those of second-chance fission ($n, F = n, f + n, nf$). And at higher energies we have to take into account the third-chance fission ($n, F = n, f + n, nf + n, 2nf$) and also the ^{241}Am$(n,3n)$ mechanism. Fission barriers result from adjustments made to best match the

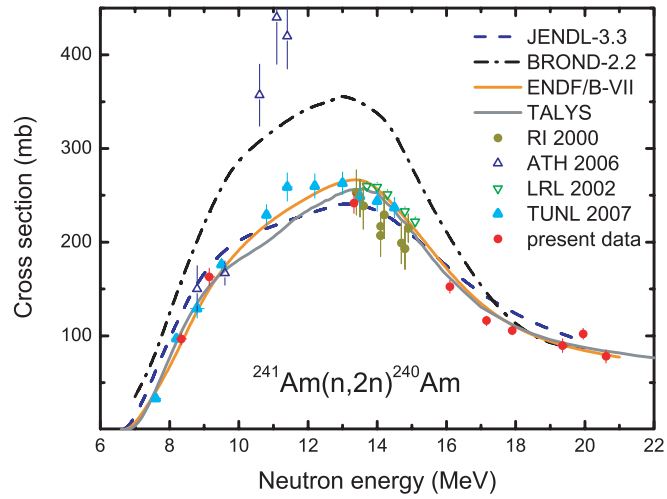

FIG. 4. (Color online) The experimental ^{241}Am$(n,2n)$ cross sections obtained at IRMM compared with previous data and evaluations.

^{241}Am(n,f) experimental data. Their magnitudes are typically around 5.9–6.2 MeV for the inner barriers and 0.2–0.5 MeV lower for the outer barriers. These values agree with theoretical predictions from Möller *et al.* [45] but, before all, they strongly depend on the compound nucleus formation cross section (i.e., from the optical potential) used in the calculations. Barriers are *de facto* uncertain to about 0.5 MeV.

The calculation of the ^{241}Am$(n,2n)$ reaction cross section constitutes a real challenge because this cross section is relatively small and totally embedded with those of all other competing processes. Nevertheless, as compared in Fig. 4, the TALYS calculations from Bruyères-le-Châtel agree accurately with our present measurements.

V. RESULTS AND DISCUSSION ON THE UNCERTAINTIES

Our results for the ^{241}Am$(n,2n)^{240}$Am reaction cross section are given in Table V and compared with existing measurements and the new model calculation in Fig. 4. Also shown are the estimates from Refs. [5–7], the ENDF/B-VII, JENDL-3.3, and BROND-2.2 evaluated data files. The first column in Table V gives the neutron energy and its spread in parentheses, the second column gives the measured cross sections, and the third column gives the total uncertainty. The correlation matrix is given in the last column.

A. Data uncertainties and their correlations

Uncertainties and the correlation matrix for the uncertainties, in case several data points are reported, are of great current interest (e.g., [46]). A careful evaluation was made by Tonchev *et al.* [4] of the uncertainties of their data for this reaction. Here an effort is made to present both uncertainties and the correlation matrix. For the activation work at IRMM, so far no explicit covariance data have been provided, although in principle a full report of the method and input uncertainties is usually given and the recipe for constructing the covariance data was detailed [35].

TABLE V. The ^{241}Am$(n,2n)^{240}$Am cross sections obtained from this work, with their total uncertainties and the degree of correlation between the different energy points.

Energy (MeV)	σ_{Am} (mb)	Uncertainty (%)	Correlation matrix (×100)								
8.34(15)	96.8	6.5	100								
9.15(15)	162.9	5.7	35	100							
13.33(15)	241.8	4.6	37	42	100						
16.10(15)	152.4	4.6	38	43	53	100					
17.16 (3)	116.1	4.4	40	45	57	58	100				
17.90(10)	105.7	4.4	41	45	57	59	84	100			
19.36(15)	89.5	8.2	21	24	30	31	39	39	100		
19.95(7)	102.1	5.8	30	34	44	45	58	59	51	100	
20.61(4)	77.9	8.8	20	22	29	30	40	42	39	65	100

The uncertainties of the cross sections with the correlation matrix as given in Table V were obtained by propagating the full covariance matrix of the components of Eq. (1). Most of the components were considered independent from each other, with the exception of several strongly related quantities for which we estimated the uncertainty of the ratio of the Am and Al measurement for each energy. The contribution of the uncertainties of the ratio to the covariance matrix was then determined.

All possible uncertainties have been evaluated, and Table VI shows only the ones above 0.1%. The other negligible ones correspond to the uncertainty on the γ-ray intensity I_γ, the decay constant λ propagated to the corresponding time factors f_Σ and f_r of the Al monitor reaction, and for the ratio $C_{\mathrm{flux,Am}}/C_{\mathrm{flux,Al}}$. The relative flux ratio $\Phi_{0,\mathrm{Al}}/\Phi_{0,\mathrm{Am}}$ was estimated within good agreement both with an analytical approximation and with Monte Carlo simulations and its uncertainty was also neglected.

Other uncertainties were uncorrelated, such as the detected counts S_{Am}, ranging from 1.4% to 6.3%, and S_{Al}, ranging from 0.7% to 2%. The factor S_{Am} forms the major source of uncertainty as a result of a low count rate due to both a large background from the ^{241}Am natural activity and a decreasing reaction cross section with energy. We used six different Am samples for nine energy points. The correlated uncertainty of 0.3% for the same sample at different energy points was taken into account. The Al samples, with an uncorrelated uncertainty on the mass of 0.1%, were different for all energy points.

TABLE VI. Uncertainties (in %) for the most significant contributions in Eq. (1) at each neutron energy. Only the diagonal elements are given. The full matrix for each component is not given here but was used to obtain the correlation matrix in Table V.

Neutron energy (MeV)	σ_{Al}	S_{Am}	S_{Al}	I_{Am}	n_{Al}	n_{Am}	$\epsilon_{\mathrm{Al}}/\epsilon_{\mathrm{Am}}$	$(f_\Sigma f_r)_{\mathrm{Am}}$	$\frac{C_{\mathrm{low,Am}}}{C_{\mathrm{low,Al}}}$
8.34	1.9	5.0	1.0	1.2	0.1	0.3	3.0	0.9	
9.15	1.9	4.0	1.0	1.2	0.1	0.3	3.0	0.6	
13.33	1.6	2.5	1.0	1.2	0.1	0.3	3.0	0.4	0.3
16.1	2	2.1	1.0	1.2	0.1	0.3	3.0	0.6	0.3
17.16	2	1.5	1.0	1.2	0.1	0.3	3.0	0.6	0.3
17.9	2.2	1.3	0.7	1.2	0.1	0.3	3.0	0.7	0.3
19.36	3.1	6.3	2.0	1.2	0.1	0.3	3.0	0.6	1.3
19.95	4.1	1.4	1.0	1.2	0.1	0.3	3.0	0.6	1.4
20.61	5.4	5.7	1.6	1.2	0.1	0.3	3.0	0.6	1.4

The uncertainty on I_γ and λ for Am was of course common to each energy point. Their contribution to the corresponding time factors f_Σ and f_r was different for the energy points, ranging from 0.4% to 0.9%, because of the different irradiation and decay times. Their full correlation was propagated to the final covariance matrix.

We estimated the uncertainty of the ratio $C_{\mathrm{low,Am}}/C_{\mathrm{low,Al}}$ at 0.3% to 1.4% depending on the energy. This uncertainty mainly originates from the knowledge of the low component of the neutron spectrum, which is different for each energy. Thus, no correlation was adopted between the energy points. For the ratio of the efficiency $\epsilon_{\mathrm{Am}}/\epsilon_{\mathrm{Al}}$, the uncertainty was estimated at 3% based on a comparison of Monte Carlo simulations and point source measurements. A full correlation for the energy points was adopted. The uncertainties and correlations for the aluminum cross section σ_{Al} were taken from Ref. [17].

The final covariance matrix, giving the correlation between the energy bins, was calculated by combining all the partial covariance matrices, of which the diagonal elements for the most significant contributions are given in Table VI. The final covariance matrix was split into a vector of diagonal uncertainties, ranging from 4.4% to 8.8%, and a correlation matrix, given in Table V.

B. Discussion of the results

Of the nine cross sections obtained in this work, three can be compared with data from earlier measurements. These three data points at the neutron energies of 8.34, 9.15, and 13.33 MeV are in excellent agreement with the recent data from Tonchev *et al.* [4]. The present result at $E_n = 9.15$ MeV can further be compared with the data from Perdikakis *et al.* [3] and is in similar good agreement. The point at $E_n = 13.33$ MeV agrees well with the data from Filatenkov *et al.* [1] and is within two standard deviations below the data from Lougheed *et al.* [2]. Unfortunately, the 7-MV Van de Graaff accelerator at IRMM does not allow measurements with neutrons in the energy range of 10 to 13 MeV, so it is not possible to contribute to an understanding of the differences between Refs. [3] and [4].

Above 15 MeV, no other data are available and the six data points obtained here are the first experimental evidence for the excitation curve of this cross section. The data show a smooth behavior, although for $E_n = 19.95$ MeV a somewhat high value was obtained when compared to the two neighboring energies of 19.36 and 20.61 MeV.

As already mentioned, the consistent physics modeling of the calculation described in the previous section led to excellent agreement with the new data (Fig. 4, curve labeled TALYS). A similar effort was made recently for the ENDF/B-VII evaluation [5] using another code system but the same database. Again very good agreement is shown with the present data. Of the two earlier evaluations, JENDL-3.3 [6] agrees reasonably well, overshooting the data somewhat above 15 MeV and below 9 MeV, whereas BROND-2.2 [7] only is close to the present work above 18 MeV, showing significantly higher values than most of the data in the entire range. It is gratifying to find that consistent physics modeling and an adequate amount of data for competing channels by which to tune model parameters allows predictions for the ^{241}Am$(n,2n)$ cross section that agree so well with experiments. In this respect, it must be noted that all calculations were made before the present data and that of Tonchev *et al.* [4] were available.

VI. CONCLUSION

Cross-section measurements of the reaction ^{241}Am$(n,2n)^{240}$Am were performed for nine energies between 8.34 and 20.61 MeV using the activation technique with a quasi-mono-energetic neutron beam provided by the Van de Graaff accelerator of the IRMM. The full covariance matrix is given along with the results. This experiment extends for the first time the knowledge of this excitation function above 15 MeV. Below 15 MeV, three data points were obtained that agree very well with recent experimental work [1–4]. Excellent agreement was found with model calculations using the code TALYS. For the latter, a complete physics model was used with a dispersive phenomenological optical model developed at the Commissariat à L'Energie Atomique and detailed tuning of the model parameters to the available experimental data.

ACKNOWLEDGMENTS

We are indebted to the Van de Graaff operating team for the optimum conditions during the measurements. We also thank R. Jaime Tornin from the IRMM technical staff, and C. Brossard and M. Holzhäuser from the ITU technical staff for their contribution to the sample preparation and the measurement setup. This experiment was supported by the European Commission within the Sixth Framework Programme of EURATOM through the Transnational Access project NUDAME (Neutron Data Measurements at IRMM, Contract No. FP6-516487).

[1] A. A. Filatenkov and S. V. Chuvaev, Phys. At. Nucl. **63**, 1504 (2000).
[2] R. W. Lougheed, W. Webster, M. N. Namboodiri, D. R. Nethaway, K. J. Moody, J. H. Landrum, R. W. Hoff, R. J. Dupzyk, J. H. McQuaid, R. Gunnink *et al.*, Radiochim. Acta **90**, 833 (2002).
[3] G. Perdikakis, C. T. Papadopoulos, R. Vlastou, A. Lagoyannis, A. Spyrou, M. Kokkoris, S. Galanopoulos, N. Patronis, D. Karamanis, C. Zarkadas *et al.*, Phys. Rev. C **73**, 067601 (2006).
[4] A. P. Tonchev, C. T. Angell, M. Boswell, A. S. Crowell, B. Fallin, S. Hammond, C. R. Howell, A. Hutcheson, H. J. Karwowski, J. H. Kelley *et al.*, Phys. Rev. C **77**, 054610 (2008).
[5] M. B. Chadwick, P. Obložinský, M. Herman *et al.*, Nucl. Data Sheets **107**, 2931 (2006).
[6] K. Shibata, T. Kawano, T. Nakagawa, O. Iwamoto, J. Katakura, T. Fukahori, S. Chiba, A. Hasegawa, T. Murata, H. Matsunobu *et al.*, J. Nucl. Sci. Technol. **39**, 1125 (2002).
[7] A. I. Blokhin, T. S. Belanova, and V. M. Maslov, BROND-2.2 evaluated data file for ^{241}Am, 1990; see Ref. [9].
[8] A. Koning, R. Forrest, M. Kellett, R. Mills, H. Henriksson, and Y. Rugama, Organisation for Economic Co-operation and Development, Nuclear Energy Agency, JEFF Report No. 21, NEA No. 6190, 2006.
[9] National Nuclear Data Center Online Data Service, Evaluated Nuclear Data File database, (2007). [http://www.nndc.bnl.gov/exfor7/endf00.htm].
[10] A. J. Koning and M. C. Duijvestijn, Nucl. Instrum. Methods Phys. Res. B **248**, 197 (2006).
[11] A. Koning, S. Hilaire, and M. Duijvestijn, in *Proceedings of the International Conference on Nuclear Data for Science and Technology—ND2007* (EDP Sciences, Paris, 2008) Vol. 1, p. 211.
[12] C. Nästren, M. Holzhäuser, A. Fernandez, C. Brossard, F. Wastin, H. Ottmar, and J. Somers, European Commission Technical Report No. JRC ITU-TN-2006/34, 2006.
[13] G. Lövestam, EC-JRC IRMM Internal Report No. GER/NP/2/2002/06/20, 2002 (unpublished); [http://irmm.jrc.ec.europa.eu/html/about_IRMM/laboratories/The_Van_de_Graaff_laboratory.htm].
[14] G. Lövestam, C. Chaves, M. Conti, T. Gamboni, and R. Jaime, European Commission, Joint Research Centre, Institute for Reference Materials and Measurements, Neutron Physics Unit Scientific Report, 2002 (unpublished); [http://irmm.jrc.ec.europa.eu/html/publications/technical_reports/publications/EUR20684.pdf].
[15] H. Liskien and A. Paulsen, Nucl. Data Tables **11**, 569 (1973).
[16] H. H. Andersen and J. F. Ziegler, *Hydrogen Stopping Powers and Ranges in All Elements* (Pergamon, New York, 1977).
[17] M. Wagner, H. Vonach, A. Pavlik, B. Strohmaier, S. Tagesen, and J. Martinez-Rico, *Evaluation of Cross Sections for 14 Important Neutron Dosimetry Reactions*, Physics Data, Vol. 13-5 (Fachinformationszentrum Karlsruhe, Germany, 1990), p. 5.
[18] H. Vonach, in *Nuclear Data Standards for Nuclear Measurements, 1991 NEAND/INDC Nuclear standards file*, edited by H. Condé, Nuclear Energy Agency, Organisation for Economic Co-operation and Development, Report NEAND-311 "U",

INDC(SEC)-101 (OECD Publications, 2 rue André-Pascal, 75775 Paris Cedex 16, 1992), p. 75.
[19] D. L. Smith, A. J. M. Plompen, and V. Semkova, *Correction for Low Energy Neutrons by Spectral Indexing*, International Evaluation Cooperation, Vol. 19, NEA/WPEC-19, p. 155, Nuclear Energy Agency (Organisation for Economic Co-operation and Development, Paris, France 2005).
[20] A. B. Smith, Argonne National Laboratory Report No ANL/NDM-115, 1990 (unpublished); [http://www.td.anl.gov/reports].
[21] V. McLane, Evaluated Nuclear Data File, Sec. B, Version VI (ENDF/B-VI), National Nuclear Data Center, Brookhaven National Laboratory (unpublished); [http://www.nndc.bnl.gov/nndc/endf].
[22] R. B. Firestone, Nucl. Data Sheets **108**, 2319 (2007).
[23] P. M. Endt, Nucl. Phys. A **633**, 1 (1998).
[24] H. Junde, Nucl. Data Sheets **86**, 315 (1999).
[25] J. Blachot, Nucl. Data Sheets **104**, 967 (2005).
[26] C. M. Baglin, Nucl. Data Sheets **91**, 423 (2000).
[27] M. R. Bhat, Nucl. Data Sheets **80**, 789 (1997).
[28] G. Audi, A. H. Wapstra, C. Thibault, J. Blachot, and O. Bersillon, Nucl. Phys. A **729**, 337 (2003).
[29] B. Singh and E. Browne, Nucl. Data Sheets **109**, 2439 (2008).
[30] M. S. Basunia, Nucl. Data Sheets **107**, 2323 (2006).
[31] X-5 Monte Carlo Team, MCNP—A General Monte Carlo N-Particle Transport Code, Version 5 (Los Alamos National Laboratory, Los Alamos, NM, April 24, 2003).
[32] B. Jäckel, W. Westmeier, and P. Patzelt, Nucl. Instrum. Methods Phys. Res. A **261**, 543 (1987).
[33] K. Debertin and R. G. Helmer, *Gamma- and X-ray Spectrometry with Semiconductor Detectors* (North Holland, Amsterdam, 1988).
[34] Evaluated Nuclear Structure Data File (ENSDF), National Nuclear Data Center, Brookhaven National Laboratory, 1998.
[35] A. Fessler, A. J. M. Plompen, D. L. Smith, J. W. Meadows, and Y. Ikeda, Nucl. Sci. Eng. **134**, 171 (2000).
[36] P. Reimer, M. Hult, A. J. M. Plompen, P. N. Johnston, V. Avrigeanu, and S. M. Qaim, Nucl. Phys. A **705**, 265 (2002).
[37] P. Reimer, V. Avrigeanu, S. V. Chuvaev, A. A. Filatenkov, T. Glodariu, A. Koning, A. J. M. Plompen, S. M. Qaim, D. L. Smith, and H. Weigmann, Phys. Rev. C **71**, 044617 (2005).
[38] P. Reimer, A. J. Koning, A. J. M. Plompen, S. M. Qaim, and S. Sudár, Nucl. Phys. A **815**, 1 (2009).
[39] MCNPX version 2.5.f: Monte Carlo N-Particle transport code system for multiparticle and high-energy applications.
[40] S. Cabral, G. Börker, H. Klein, and W. Mannhart, Nucl. Sci. Eng. **106**, 308 (1990).
[41] P. Romain and J.-P. Delaroche, in *Proceedings of the NEA Specialists' Meeting on the Nucleon-Nucleus Optical Model up to 200 MeV* (Organisation for Economic Co-operation and Development, Paris, 1997), p. 167.
[42] B. Morillon and P. Romain, Phys. Rev. C **70**, 014601 (2004).
[43] M. L. Jiménez, B. Morillon, and P. Romain, Ann. Nucl. Energy **32**, 195 (2005).
[44] B. Morillon, H. Duarte, and P. Romain, AIP Conf. Proc. **1175**, 79 (2009).
[45] P. Möller, J. Nix, W. Myers, and W. Swiatecki, At. Data Nucl. Data Tables **59**, 185 (1995).
[46] T. Kawano, P. Talou, P. G. Young, G. Hale, M. B. Chadwick, and R. C. Little, Nucl. Data Sheets **109**, 2817 (2008).